Sonoporation by Single-Shot Pulsed Ultrasound with Microbubbles Adjacent to Cells

Nobuki Kudo,* Kengo Okada, and Katsuyuki Yamamoto
Graduate School of Information Science and Technology, Hokkaido University, Sapporo, Japan

ABSTRACT In this article, membrane perforation of endothelial cells with attached microbubbles caused by exposure to single-shot short pulsed ultrasound is described, and the mechanisms of membrane damage and repair are discussed. Real-time optical observations of cell-bubble interaction during sonoporation and successive scanning electron microscope observations of the membrane damage with knowledge of bubble locations revealed production of micron-sized membrane perforations at the bubble locations. High-speed observations of the microbubbles visualized production of liquid microjets during nonuniform contraction of bubbles, indicating that the jets are responsible for cell membrane damage. The resealing process of sonoporated cells visualized using fluorescence microscopy suggested that Ca^{2+}-independent and Ca^{2+}-triggered resealing mechanisms were involved in the rapid resealing process. In an experimental condition in which almost all cells have one adjacent bubble, 25.4% of the cells were damaged by exposure to single-shot pulsed ultrasound, and 15.9% (~60% of the damaged cells) were resealed within 5 s. These results demonstrate that single-shot pulsed ultrasound is sufficient to achieve sonoporation when microbubbles are attached to cells.

INTRODUCTION

Sonoporation is a transient increase in cell membrane permeability (1,2) caused by cavitation phenomena (3,4) during exposure to ultrasound. Sonoporation is of potential use as a method for gene delivery and drug delivery, and its efficiency is enhanced by the presence of microbubbles (5,6). In almost all cases, sonoporation has been carried out using continuous or long-burst ultrasound. These exposure conditions are essential for achieving high efficiency of sonoporation but have adverse effects on biological tissue. On the other hand, in vivo use of microbubbles as an ultrasound contrast agent is now very common, and many studies have shown the usefulness of microbubbles for improving the efficiency of in vivo sonoporation (7), indicating the possibility of efficient in vivo sonoporation using less harmful ultrasound in the presence of microbubbles. It has been reported that exposure to ultrasound pulses from diagnostic ultrasound equipment can cause sonoporation when associated with microbubbles (8,9). The mechanisms by which microbubbles cause sonoporation of cell membranes have been revealed by high-speed observation of microbubble behavior (10–12) and cell-bubble interaction (13–17); however, there have been few studies on repair of damaged cell membranes (15,18,19), and the entire sonoporation process from membrane damage to repair has not been elucidated.

To elucidate the entire mechanisms of sonoporation, we studied sonoporation of cells exposed to single-shot pulsed ultrasound of a few microseconds in duration in the presence of adjacent microbubbles. Because little radiation force and acoustic streaming are produced, this exposure condition enables direct microscopic observations of single cell dynamics during sonoporation. To determine the mechanism by which cell membrane permeability is increased, cells were also observed using a scanning electron microscope (SEM), and the behavior of microbubbles was observed using a high-speed camera. Furthermore, to determine the mechanisms of cell membrane repair, the dynamic process of membrane repair was examined using live-cell fluorescence microscopy.

MATERIALS AND METHODS

Real-time observation of cell membrane damage using a light microscope

In our experiments, bovine endothelial monolayer cells with microbubbles attached were exposed to single-shot pulsed ultrasound under light microscopic observation, and cell membrane damage was also observed using an SEM. An inverted-type microscope (IX70, Olympus, Tokyo, Japan) was used in all experiments, and phase-contrast and fluorescent images were captured using a digital camera (C-5050, Olympus) or a video camera (GR-X5, Victor, Tokyo, Japan). An observation chamber for maintaining target cells and bubbles in the field of view was created in the bottom plate of a water bath placed on the microscope stage (Fig. 1, *a* and *b*). The observation chamber was sandwiched with glass coverslips (C218181, Matsunami Glass Industry, Osaka, Japan) from the top and bottom sides and filled with Hanks' balanced salt solution (HBSS) supplemented with 5 μg/ml propidium iodide (PI), which permeates only through damaged cell membranes and produces red fluorescence. The solution was also supplemented with the ultrasound contrast agent Levovist (Schering AG Medical, Berlin, Germany), which contains microbubbles of ~1 μm in diameter. We used this agent considering that particularly small sizes of the bubbles would minimize cell membrane damage and maximize repair. In this condition, the microbubbles are suspended just beneath the surface of the upper coverslip, and the presence of this rigid glass wall adjacent to the bubbles influences the dynamics of bubble collapse. Densities of cells and bubbles were ~50–200 /mm^2 (~5–10% confluent) and 1000–3000 /mm^2,

Submitted May 9, 2008, and accepted for publication February 3, 2009.

*Correspondence: kudo@bme.ist.hokudai.ac.jp

Editor: Richard E. Waugh.

0006-3495/09/06/4866/11 $2.00

doi: 10.1016/j.bpj.2009.02.072

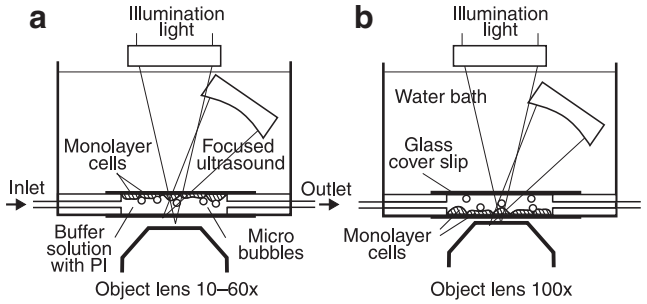

FIGURE 1 Experimental setup of an observation chamber for real-time visualization of the sonoporation process using a light microscope. Observation using a 10–60× objective lens (*a*) and a 100× objective lens (*b*).

respectively. Densities of bubbles were controlled by changing waiting time for suspended bubbles to rise toward the surface so that almost all cells observed in a field of view had one adjacent bubble at the time of ultrasound exposure. Waiting time was decided by visual inspection of numbers of cells and bubbles and was in the range of 10–30 min.

A laboratory-assembled focused transducer (aperture, = 50 mm; focal length, 70 mm) was driven by a three-cycle sinusoidal wave of 1 MHz in center frequency. Pressure measurement was carried out using a polyvinylidene difluoride membrane hydrophone (MHA500B, NTR Systems, Seattle, WA) in the absence of the observation chamber. Peak positive and negative pressures at the focus were 8.0 and −1.1 MPa, respectively (15). Asymmetry in these peak pressures is caused by combined effects of nonlinear propagation of focused ultrasound in water and diffraction associated with finite size of the transducer (20). In the practical condition with the observation chamber at the focus, reflection of ultrasound at the upper coverslip decreases ultrasound pressure applied to cells. This effect was, however, minimized by using coverslips of 0.16 mm in thickness, which corresponds to ~1/40 of the ultrasound wavelength. In fact, magnitudes of decrease in peak positive and negative pressures measured in the presence of a glass coverslip at the focus were 34% and 14%, respectively, when ultrasound was irradiated at the angle of 45° to the coverslip. Although nearly complete reflection due to the glass-air interface occurs at the lower coverslip, the reflected ultrasound beam is thought to have little effect on bubbles or cells within the field of view at the upper coverslip. The reason for this is that the incident beam of ultrasound, the incident angle of which is ~45°, causes mirror reflection at the lower coverslip and the beam is sufficiently far from the field of view when the reflected beam reaches the upper coverslip because the space between the upper and lower coverslips (1.5 mm) is much greater than the size of the field of view. The same exposure condition of ultrasound was used in all experiments to observe cell membrane damage.

In observations using 10× (UPlanFI 10XPH; numerical aperture (NA) = 0.3, working distance (WD) = 10 mm; Olympus), 40× (SLCPlanFI 40XPH; NA = 0.55, WD = 6.4–8.3 mm; Olympus) and 60× (LCPlanFI 60XPH; NA = 0.7, WD = 1.7 mm; Olympus) objective lenses, a glass coverslip seeded with bovine endothelial monolayer cells was attached to the top side of the observation chamber with the cultured cells face down so that the bubbles coming up to surface by buoyancy force could make contact with them (Fig. 1 *a*). In observation using a 100× objective lens (UPLFLN 100XO2PH; NA = 1.3, WD = 0.2 mm; Olympus), a coverslip with cultured cells was mounted on the bottom side of the observation chamber with the cells face up (Fig. 1 *b*), because of the short working distance of the lens. To make bubbles come into contact with cells, first, the observation chamber was filled with a microbubble suspension and then the water bath was placed upside down for longer than 20 min. In this arrangement, the bubbles in the observation chamber propelled upward by buoyancy force and could make contact with the cells. After that, the water bath was returned to the original position, and the cells with attached microbubbles were used for observation.

Confirmation of cell membrane damage using an SEM

For further exploration on cell membrane damage, observation was also carried out using an SEM. Cells on a coverslip with microbubbles attached were exposed to single-shot pulsed ultrasound under light microscopic observation with a 40× objective lens. Five seconds after exposure, the solution inside the observation chamber was replaced with 2% glutaraldehyde via inlet and outlet tubes (Fig. 1 *a*). To protect cells from excess pressure and shearing force, injection of the fixative and ejection of the solution were manually performed synchronously. A fluorescence image of PI was taken just before the injection of the fixative. After several hours, the coverslip with the fixed cells was removed from the observation chamber and prepared for SEM observation using the t-butyl alcohol freeze-drying method (21). The processed sample was then observed using an SEM (JSM-5100 or JSM-5300, JEOL, Tokyo, Japan) operating at 20–25 kV. Many cells were scanned by the SEM until the same cell as that observed by the light microscope was found. To decrease the number of cells that had to be searched, we used 5–10% confluent cell samples.

Bubble dynamics observed using a high-speed camera

To elucidate the mechanisms underlying membrane perforation by sonication with Levovist bubbles, behavior of the microbubbles under exposure to single-shot pulsed ultrasound was observed using a high-speed camera (Ultranac, Nac Image Technology, Tokyo, Japan) equipped to the microscope. Frame rates were set to 4–16 MHz, and 24 frames were taken at one time. Two types of larger bubbles were also used in these experiments: albumin-shelled microbubbles of ~20 μm in diameter and bubbles of the ultrasound contrast agent Optison (GE Healthcare, Princeton, NJ) of ~3 μm in diameter. These larger bubbles were used to assist examination of the dynamics of Levovist bubbles because high-speed observation of Levovist bubbles in contraction phase was difficult due to their small sizes. Albumin-shelled microbubbles were prepared by agitating albumin-saline solution. The observation chamber was the same as that used for the observation of cell-bubble interaction (Fig. 1 *a*) except that no cell was seeded on a coverslip, resulting in bubbles being directly attached to the coverslip. The process of micron-sized shell-encapsulated bubble collapse is very complex, and theoretical and simulation studies have still not revealed this process. Therefore, to elucidate the collapsing process, high-speed observation was carried out under the asymmetric condition with the coverslip. The exposure condition of ultrasound was the same as that used for the observation of cell-bubble interaction, except for the albumin-shelled bubble experiments. Another laboratory-assembled transducer (aperture, = 110 mm, focal length, 100 mm) of 250 kHz in center frequency was used due to the difference in bubble size. This transducer was driven by a three-cycle sinusoidal wave, and peak positive and negative pressures were ±0.3 MPa.

Temporal analysis of membrane repair using PI and Fura-2

In this study, the cells were fixed for SEM observation 5 s after ultrasound exposure; however, many cells demonstrated PI fluorescence despite the absence of obvious membrane damage, suggesting the presence of a rapid resealing process. To explore this process, the repair of a damaged cell membrane was examined using the fluorescent dyes PI and Fura-2. After membrane damage, PI contained in the surrounding solution infiltrates into a cell and produces fluorescence by chemical reaction with nucleic acids. Because the chemical reaction causes a delay in producing fluorescence, PI was used just to check the occurrence of membrane damage and repair at 180 s after exposure to ultrasound. In contrast, there is no time delay in production of fluorescence by Fura-2 because this dye produces fluorescence by itself without chemical reaction. Because Fura-2 trapped inside a cell drains away only in the case of membrane damage, the dynamic

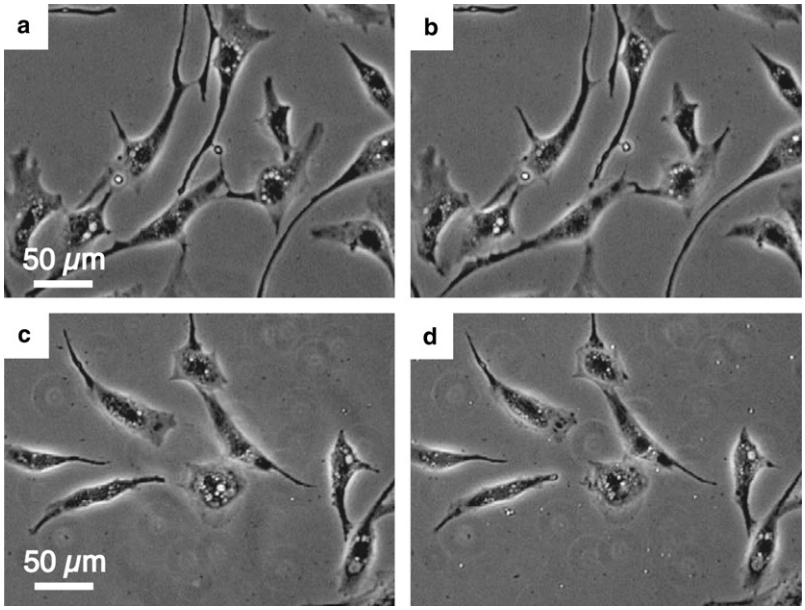

FIGURE 2 Light microscopic observation in two control conditions: before (*a*) and after (*b*) ultrasound exposure without bubble addition. Before (*c*) and after (*d*) injection of bubble suspension without ultrasound exposure.

process of membrane damage and repair can be evaluated by monitoring temporal changes in Fura-2 fluorescence intensity.

Cells cultivated on a glass coverslip were loaded with Fura-2/AM by incubation in HBSS containing 4-μM Fura-2/AM for 30 min at 37°C. The coverslip was then rinsed with HBSS and attached to the observation chamber filled with a bubble-suspended solution supplemented with 5 μg/ml PI. The wavelength of Fura-2-excitation was set to 360 nm and fluorescence was observed at 520 nm, as this enabled the Fura-2 concentration to be determined regardless of the Ca^{2+} concentration. Fluorescence of Fura-2 was videotaped starting immediately before ultrasound exposure until 120 s after exposure using a 40× objective lens. Temporal changes in Fura-2 fluorescence were evaluated in an off-line process using the video footage with photobleaching correction. Static images of PI fluorescence were photographed before and after (180 s after exposure) Fura-2 observation.

Effects of Ca^{2+} on membrane repair evaluated using PI

Cells are known to have rapid resealing mechanisms to protect themselves against lethal damage. Self-sealing of a lipid bilayer (22), which is Ca^{2+}-independent, and patching with fused intracellular vesicles (23–25), which is Ca^{2+}-triggered, are known to play important roles in rapid resealing. To explore the mechanisms in our sonoporation model, we examined the rates of damaged cells under the following three conditions: cells were attached to the observation chamber filled with HBSS containing 1.3 mM Ca^{2+} and supplemented with PI before ultrasound exposure; cells were attached to the observation chamber filled with HBSS containing Ca^{2+} and supplemented with PI 120 s after ultrasound exposure; and cells were attached to the observation chamber filled with Ca^{2+}-free phosphate-buffered salt solution (PBS) and supplemented with PI 120 s after ultrasound exposure. Basically, the rate of membrane damage in each condition was determined from the number of total and PI-stained cells before and after ultrasound exposure under a 10× objective lens. In the first condition, all of the damaged cells were stained by PI. However, the numbers of PI-stained cells in the second and third conditions decreased by the numbers of cells that had been repaired during the 120-s period. Thus, the rate of repair in each condition with and without Ca^{2+} was obtained from the rate of membrane damage in the second or third condition subtracted from that in the first condition. In this experiment, we considered that the rate of cell membrane damage does not depend on Ca^{2+} concentration of the solution. Even under a physiological condition with extracellular Ca^{2+} concentration of 1–2 mM, intracellular Ca^{2+} concentration is maintained at 50–100 nM. Therefore, it was thought that short incubation of cells in Ca^{2+}-free solution does not change the physiological condition of cells and, therefore, also does not change physical properties of the cell membrane. To confirm this, another set of experiments was carried out to evaluate rates of membrane damage immediately after ultrasound exposure in the presence and absence of Ca^{2+}.

RESULTS

Cell membrane damage at the bubble location

Control studies were carried out to examine effects of ultrasound exposure without bubble addition and bubble addition without ultrasound exposure. Phase-contrast and PI-fluorescence images were obtained using a 10× objective lens before and after ultrasound exposure or bubble addition. Fig. 2 shows images clipped from the obtained phase-contrast images. Fig. 2, *a* and *c*, shows cells before ultrasound exposure and bubble addition, respectively. Initially, fluorescence of PI was not observed in any of the cells. After exposure to one-shot pulsed ultrasound, neither cell deformation (Fig. 2 *b*) nor PI fluorescence was observed. The same result was also obtained in the case of bubble suspension being injected via the inlet and outlet tubes (Fig. 2 *d*). In the entire fields of view, generation of PI fluorescence was observed in 0% of the cells exposed to ultrasound (0/133) and in 0% of the cells with bubble addition (0/90).

Fig. 3, *a–c*, shows frames from real-time film footage (see Movie S1 in the Supporting Material) of cell-bubble interactions observed using a 40× objective lens. The bubbles that were observed before the ultrasound pulse (Fig. 3 *a*) immediately disappeared upon exposure to the ultrasound (Fig. 3 *b*). At this time, perforation occurred at the sites where the bubbles had been located. Ten minutes after ultrasound exposure, cell deformation was still observed (Fig. 3 *c*), and the appearance of strong PI fluorescence suggested that the cell

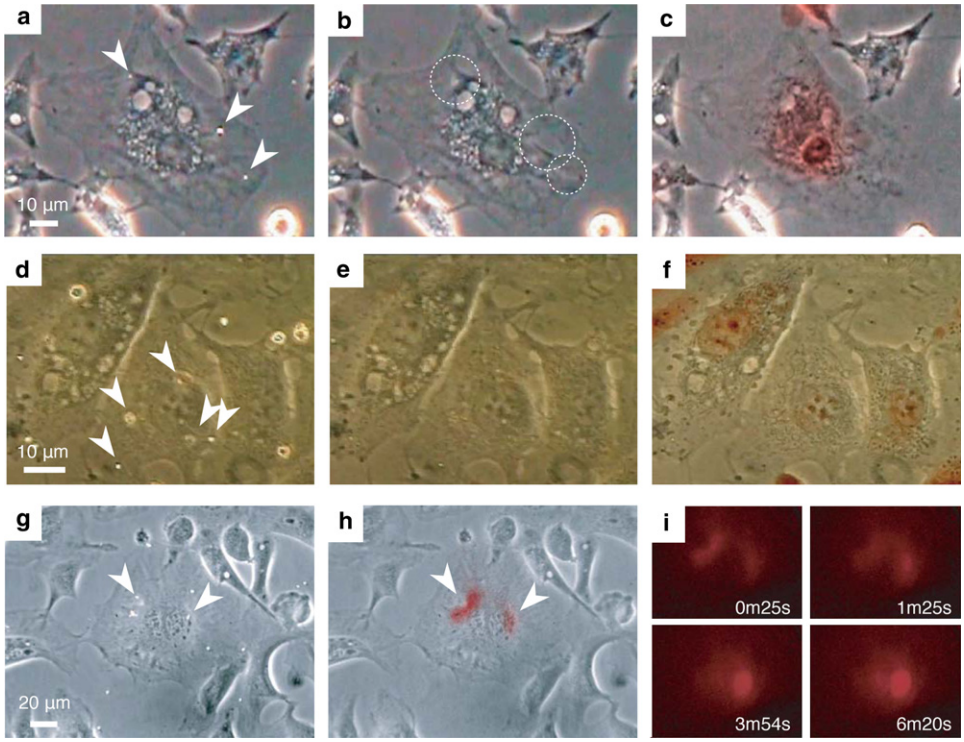

FIGURE 3 Frames from real-time film footage of cell-bubble interactions. (*a*) Observation with a 40× objective lens before ultrasound exposure revealed three microbubbles (*arrowheads*) attached to an endothelial cell. (*b*) When the cell was exposed to single-shot pulsed ultrasound, the bubbles disappeared, leaving three pits. (*c*) Extensive PI fluorescence was observed 10 min after ultrasound exposure. (*d*) Observation using a 100× objective lens before ultrasound exposure revealed five microbubbles (*arrowheads*) attached to the cell in the center of the field. (*e*) Immediately after exposure, no obvious damage was visible at the sites of the bubbles. (*f*) Two minutes after exposure, faint PI fluorescence was observed. (*g*) Observation with a 60× objective lens before ultrasound exposure. (*h*) At 25 s after exposure, PI fluorescence was observed in areas adjacent to two bubbles (*arrowheads*). (*i*) Sequential images of PI fluorescence, which were taken at 25 s, 1 min 25 s, 3 min 54 s, and 6 min 20 s after exposure to ultrasound, indicate the spread of fluorescence originating from the bubble position.

had been lethally damaged (Fig. 3 *c*; red fluorescence superimposed on a phase-contrast image). Movie S2 is another film footage of a cell with severe membrane damage. However, membrane damage was not always apparent under a light microscope. Fig. 3, *d–f*, also shows frames selected from real-time film footage but observed using a 100× objective lens. Despite high spatial resolution, no perforation was observed (Fig. 3 *e*). However, PI fluorescence suggests the presence of optically invisible perforation (Fig. 3 *f*). Temporal changes in PI fluorescence are shown in Fig. 3, *g–i*. Microbubbles disappeared when cells were exposed to ultrasound, and fluorescence of PI was observed only in the area adjacent to two bubbles indicated by white arrowheads (Fig. 3 *h*, 25 s after exposure). As shown in the sequential fluorescent images (Fig. 3 *i*), PI diffused into the cytoplasm with time (1 min 25 s after exposure), and strong fluorescence was observed when PI reached the nucleus containing a high concentration of nuclear acid (3 min 54 s and 6 min 20 s after exposure).

Fig. 4 shows light microscopic and SEM images of cells observed in three control conditions: neither ultrasound exposure nor bubble addition (Fig. 4 *a*), ultrasound exposure without bubble addition (Fig. 4 *b*), and bubble addition without ultrasound exposure (Fig. 4 *c*). Fluorescence of PI was not observed in any of the conditions, and phase-contrast images are shown in Fig. 4. In SEM images, there was no obvious change in cell shapes from those in optical images, suggesting that exposure to ultrasound pulse or injection of bubble suspension into the observation chamber does not cause membrane damage. Furthermore, even in the case with a microbubble on the cell membrane, no vestige was found at the bubble location (*arrowhead*, Fig. 4 *c*), indicating that the presence of bubbles on the cell membrane also does not cause membrane damage. On the other hand, regardless of the condition, cells showed an irregular surface with dimples and wrinkles, suggesting distinguishing cells with membrane damage only from their shapes is difficult.

Fig. 5 shows optical and SEM images obtained before and after ultrasound exposure of two cells. Levovist microbubbles attached to cell membranes (Fig. 5, *a* and *f*) disappeared after exposure to single-shot pulsed ultrasound (Fig. 5, *b* and *g*). No membrane damage was visible in the phase-contrast images, but the appearance of PI fluorescence indicated that cell membrane perforation had occurred. SEM images of the same cells revealed a small perforation at the location of the bubble (Fig. 5, *c* and *h*, *yellow box*). High-magnification views of the bubble locations showed perforations with diameters of ~1 μm, surrounded by a rough surface with small pores (Fig. 5, *d* and *i*). The SEM images also revealed the presence of perforation-like structures not at the location of bubbles (Fig. 5, *c* and *h*, *blue box*). Because high-magnification views at these locations showed apparently different characteristics (Fig. 5, *e* and *j*), these structures are thought to be inherent structures of the cell membrane or artifacts produced during the process of preparation for SEM observation. This result means that knowledge of adjacent bubble location is essential for identifying membrane damage caused by sonoporation.

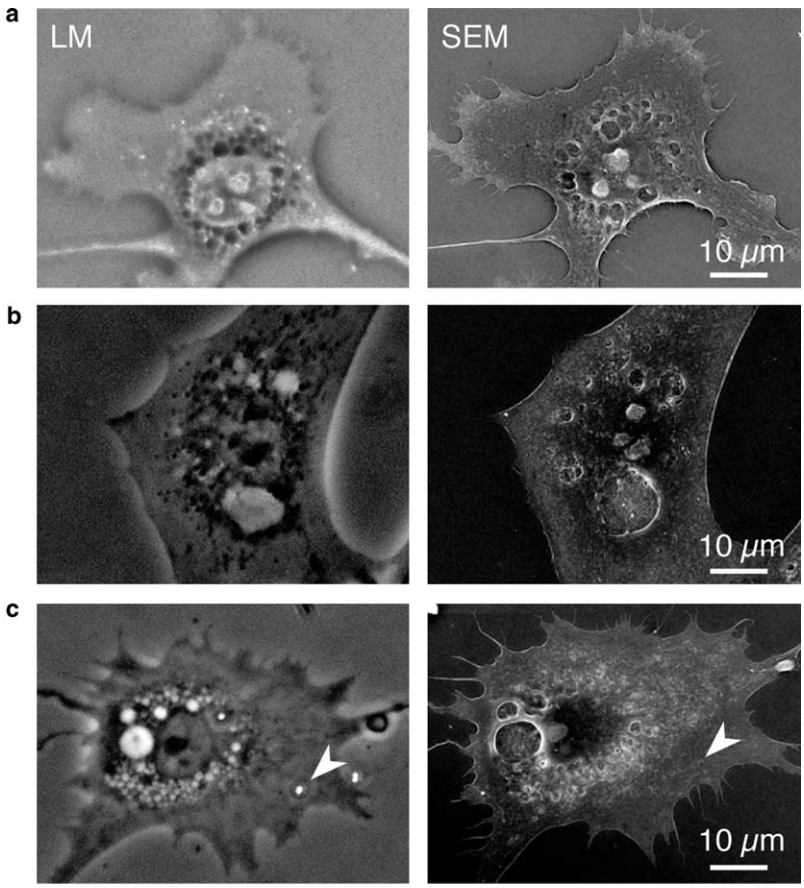

FIGURE 4 Light microscopic (LM) and SEM observation of cell membrane damage in three control conditions: neither ultrasound exposure nor bubble addition (*a*), ultrasound exposure without bubble addition (*b*), and bubble addition without ultrasound exposure (*c*).

Bubble behavior under single-shot pulsed ultrasound

Twenty-four frames were taken in the high-speed photography, and selected frames are shown in Fig. 6. Fig. 6 *a* shows behavior of an albumin-shelled microbubble of 20 μm in diameter. Deformation from a spherical bubble to ring bubble, known as a vortex ring (26,27), was observed during the contraction phase. Because a vortex ring is produced in the presence of a flow that penetrates the center of the ring, this observation indicates that the flow was produced against the coverslip during nonuniform bubble contraction. Fig. 6 *b* shows another type of nonuniform contraction of an Optison bubble of ~3 μm in diameter. In this case, after expansion to ~10 times of its initial diameter, the bubble showed nonspherical shapes in the first and second contraction phases (frames #2, #3 and frames #5, #6), indicating that a bubble can undergo asymmetric contraction and jetting in directions not against the rigid wall. The behaviors of 1-μm diameter microbubbles of the ultrasound contrast agent Levovist are shown in Fig. 6, *c* and *d*. In both cases, bubbles expanded to more than 10 times their initial diameter and then collapsed to a size too small for their shapes to be recognized (frames #4); however, the bubbles showed characteristic shape changes in the reexpansion phase (frames #5). Fig. 6 *c* shows bubbles divided into three or five fragments lying on a circle (frames #5, #6), suggesting that bubble rings produced in the same way as that shown in Fig. 6 *a* were divided into these fragments. Fig. 6 *d* shows bubbles divided into two fragments. In this case, the shapes of the fragments in frames #5 and #6 were similar to those in frames #2 and #3 of Fig. 6 *b*, suggesting that these fragments were also divided by jet flows in directions not against the rigid wall.

Repair of damaged cell membrane

Fig. 7 shows damage and repair of cells evaluated by temporal changes in PI and Fura-2 fluorescence. Fig. 7 *a* shows a typical cell in a control condition in which cells were exposed to ultrasound with no bubbles. Fig. 7, *b–d*, show typical cells that belong to ''no-damage'', ''damage and repair'', and ''damage and no-repair'' groups classified according to the levels of PI staining in images #4, which show cells at 180 s after exposure to ultrasound. PI fluorescence was not observed in the control group (Fig. 7 *a*, image #4) and the no-damage group (Fig. 7 *b*, image #4) but was observed in the two damage groups. Intensity of PI fluorescence was weak in the damage and repair group (Fig. 7 *c*, image #4) because inflow of PI was stopped during membrane repair, and it was strong in the damage and no-repair group (Fig. 7 *d*, image #4) because PI persistently infiltrated into cells.

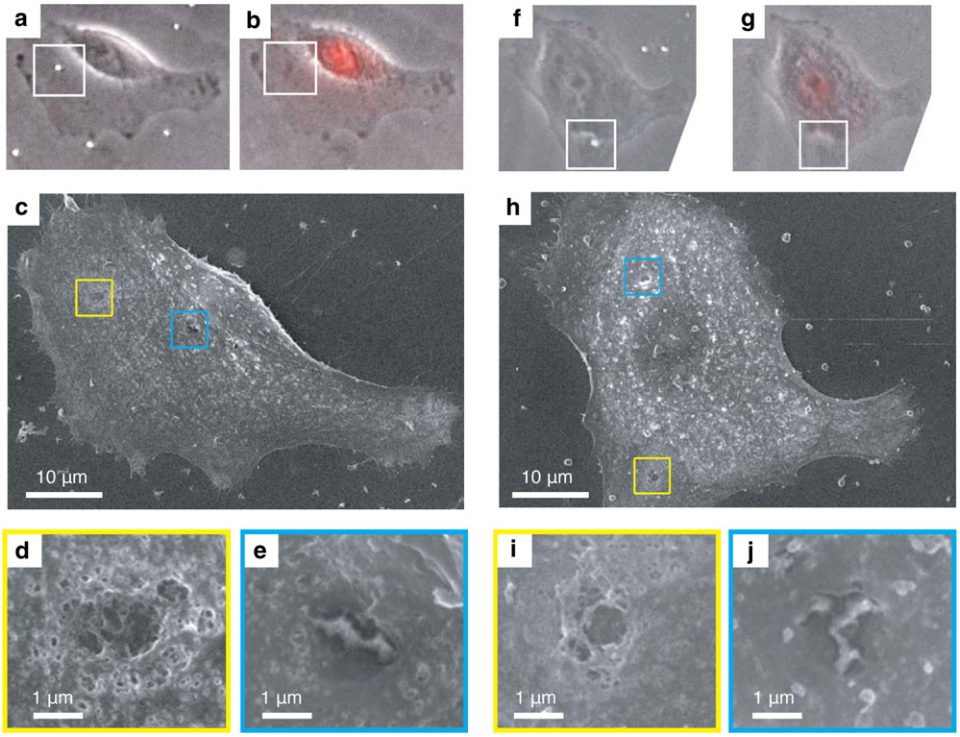

FIGURE 5 Light microscopic and SEM images of cell membrane damage. Optical images obtained before (*a* and *f*) and after (*b* and *g*) ultrasound exposure show the locations of bubbles (*boxed area*) and PI fluorescence indicating membrane damage. (*c* and *h*) SEM images of the same cells. (*d* and *i*) High-magnification views of the bubble locations (*c* and *h*, *blue box*) showing perforations of ~1 μm in diameter surrounded by a rough surface with small pores. (*e* and *j*) High-magnification views of locations with no bubbles (*c* and *h*, *yellow box*) show characteristics different from those in bubble locations.

Images #1–#3 of each group show Fura-2 fluorescence before and at 60 s and 120 s after exposure to ultrasound, respectively, and four curves shown in Fig. 7 *e* represent the average temporal changes in Fura-2 fluorescence of eight cells in each group. In the control group, no change synchronized with ultrasound exposure was observed in fluorescence intensity. In the no-damage group, the level of fluorescence transiently decreased before returning to the initial level within 120 s after exposure. In the damage and no-repair group, the fluorescence rapidly decreased immediately after exposure and slowly approached the background level. In the damage and repair group, the fluorescence also decreased rapidly, but was then maintained within ~5 s at a level significantly greater than that of the damage and no-repair group ($p < 0.01$). The time constant of the rapid decrease in average fluorescence was 2.3 s. These results suggest that membrane damage caused by exposure to pulsed ultrasound was repaired during this short period.

Effect of Ca^{2+} on membrane repair

Fig. 8 shows the percentage of damaged cells as indicated by PI uptake and fluorescence measured in the three conditions of Ca^{2+} and PI supplementation. The proportion of damaged cells before repair was 25.4 ± 5.2% (mean ± SD), and the proportions after 120 s for restoration in the presence and absence of Ca^{2+} decreased to 9.5 ± 2.7% and 19.5 ± 3.5%, respectively, indicating that 15.9% and 5.9% of cells were repaired in the presence and absence of Ca^{2+}, respectively. This means that both Ca^{2+}-independent and Ca^{2+}-triggered mechanisms were activated for resealing. Eight fields of view were assessed in each group (24 fields in total), and the average cell count in 1 field of view was 201.8 ± 51.1. Effects of the existence of extracellular Ca^{2+} on membrane damage were evaluated in another set of experiments. The proportions of damaged cells were 14.0 ± 7.5% and 13.6 ± 5.9% in the presence and absence of Ca^{2+}, respectively, showing no significant difference in cell membrane damage rates depending on the presence of Ca^{2+} ($p = 0.92$). This result confirms our assumption that short incubation of cells in Ca^{2+}-free solution does not affect damage rates of cells. The difference between the proportions (25.4% and 14.0%) is thought to be caused by differences in cell conditions (passage number, for example) and/or bubble concentration. In this experiment, 8 fields of view were assessed in each condition, and the averaged cell count in 1 field of view was 222.8 ± 83.0.

DISCUSSION

Sonoporation by single-shot pulsed ultrasound

Use of single-shot pulsed ultrasound, which causes little acoustic streaming, enabled light microscopic observation while keeping cells within a field of view during sonoporation (28). This observation showed that a single shot of pulsed ultrasound is sufficient to perforate endothelial cell membranes in the presence of microbubbles attached to the membrane (Fig. 3). Because this exposure condition is quite different from the condition that produces free radicals (29), sonochemical effects are not considered to be responsible for membrane perforation. A study by Lawrie et al. (30)

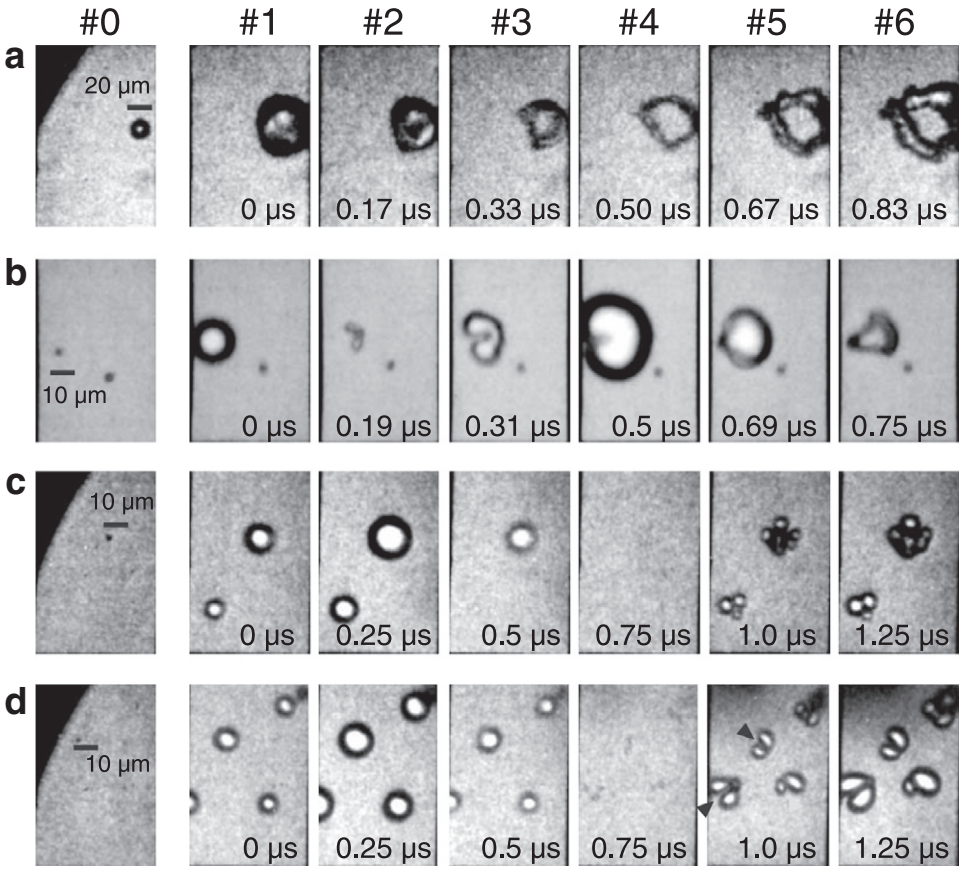

FIGURE 6 Behavior of bubbles observed at framing rates of 4–16 MHz. The first frames (#0) show bubbles in a resting condition, and the following six frames (#1–#6) show typical bubble behavior imaged with the time delay shown at the bottom of each panel. (*a*) An albumin-shelled microbubble of ~20 μm in diameter. (*b*) A bubble of the ultrasound contrast agent Optison of ~3 μm in diameter. (*c* and *d*) Bubbles of the ultrasound contrast agent Levovist of ~1 μm in diameter.

showing no dependence of gene transduction on free radical production supports our results.

In the case of conventional sonoporation for cells suspended in a medium with no bubbles, use of continuous wave or long-burst ultrasound is known to have two essential roles: one is building up cavitation nuclei to resonant-sized bubbles by rectified diffusion (31), and the other is to increase frequency of cavitation bubbles existing beside cells by the mixing effect of acoustic streaming (32). However, this condition is not essential in our sonoporation because bubbles of resonant sizes are already adjacent to cells. In the case of conventional sonoporation with microbubbles, Deng et al. (18) measured transmembrane current during sonoporation using *Xenopus oocytes* bathed in culture medium with Optison bubbles. They found that there was a distinct delay of 0.2 s for onset of transmembrane current increase and also that burst ultrasound of 0.2 s or shorter in duration could not induce transmembrane current. Also in this case, exposure to 0.2-s burst ultrasound is thought to play an essential role in bringing activated bubbles adjacent to cells.

Cell-bubble interaction was observed under the condition of cells facing up and the condition of cells facing down, causing a difference in contact condition of the bubbles to cells. In the case of cells facing up, only bubbles that had adhered to cells were observed; and in the case of cells facing down, bubbles floating beneath the cells were also observed. Despite this difference, fluorescence of PI was observed in both contact conditions, suggesting that cells in the range of jets can be perforated. This tolerance in contact condition of bubbles is meaningful because various contact conditions are possible in an in vivo situation. Production of membrane perforation only at the locations of bubbles is an important characteristic in application of bubbles targeted to specific tissue (33,34). Under exposure to continuous-wave or long-burst ultrasound, targeted bubbles might cause damage to other cells initially without attached bubbles because cavitation bubbles, which were nucleated by remnants of the targeted bubbles and scattered by blood flow or acoustic streaming, retained violent activities that cause cell damage during ultrasound exposure. The target area of sonoporation can be well controlled by selecting the position of the ultrasound beam; however, sonoporation using single-shot pulsed ultrasound is considered to achieve selectivity in a single cell basis by action of targeting bubbles.

Mechanisms of cell membrane damage

The control experiments for which results are shown in Figs. 2 and 4 indicate that exposure to ultrasound, injection of bubble suspension to the observation chamber, and presence of bubbles on cell membranes do not cause membrane damage

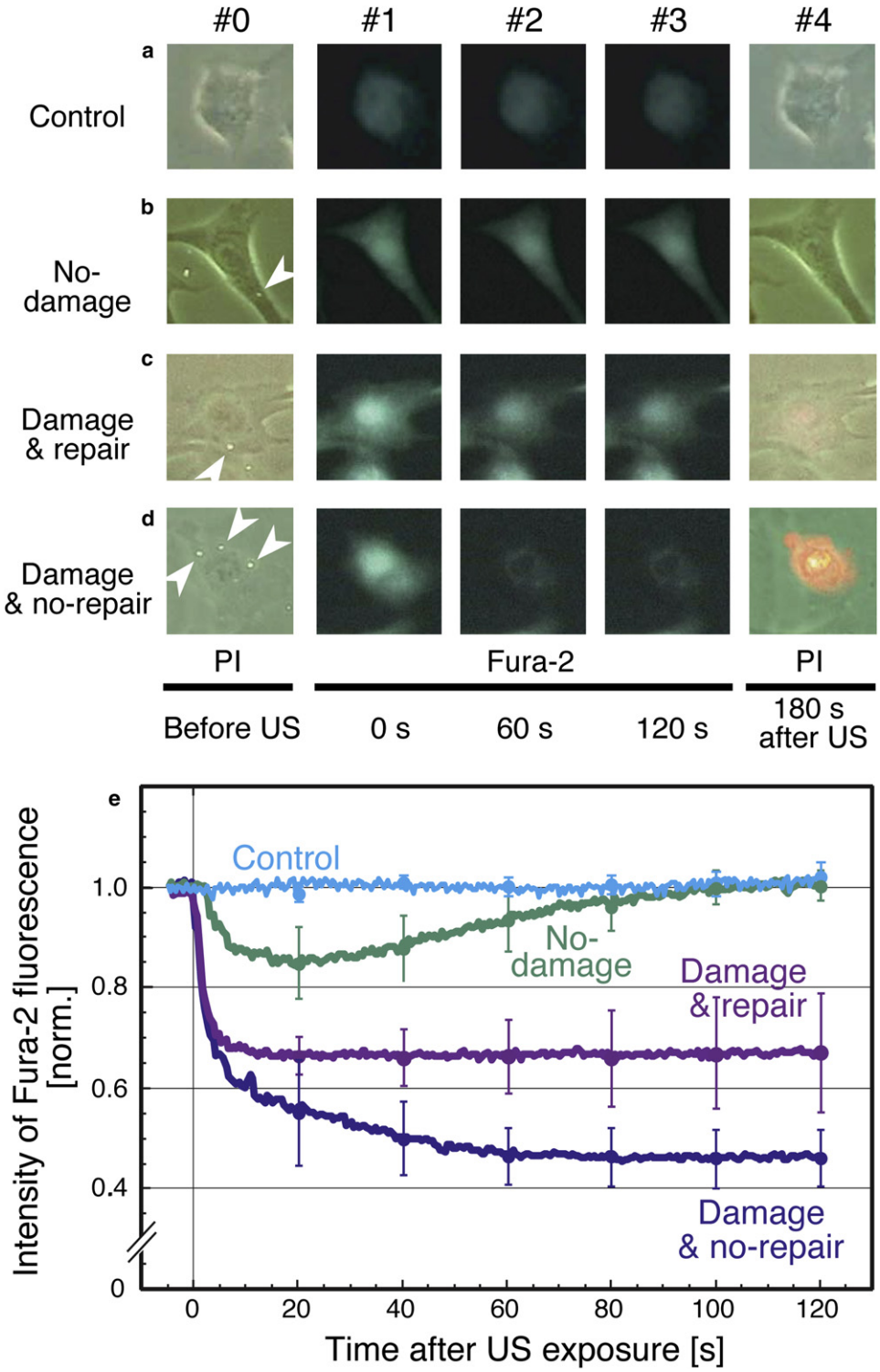

FIGURE 7 Damage and repair of a cell membrane evaluated by temporal change in PI and Fura-2 fluorescence. Images #0 and #4 show PI fluorescence images superimposed on phase-contrast images of cells taken before and 180 s after exposure to pulsed ultrasound, respectively. (*a*) A typical cell in a control condition in which cells were exposed to ultrasound without bubbles. (*b–d*) Typical cells in a condition in which cells were exposed to ultrasound with microbubbles. According to the levels of PI staining at 180 s after exposure, the cells were categorized into three groups: no damage (*b*), damage and repair (*c*), and damage and no-repair groups (*d*). Images #1–#3 in each group show Fura-2 fluorescence images of the same cells before and at 60 s and 120 s after exposure to ultrasound, respectively. (*e*) Averaged temporal change in Fura-2 fluorescence in the four groups. Error bar represents SD.

by themselves. Membrane perforation was observed only when cells were exposed to ultrasound in the presence of microbubbles attached to the cells, and the presence of membrane perforation at the location of bubbles (Fig. 3, *a–c*) suggests that this perforation is due to direct mechanical effects of bubble behavior. The finding of optically invisible micron-sized perforations at the locations of bubbles, which were detected only by SEM observation (Fig. 5), supports this idea. Furthermore, the spread of PI fluorescence originating from the bubble locations (Fig. 3 *i*) also indicates that PI infiltrated into cells via membrane perforations at the locations of bubbles.

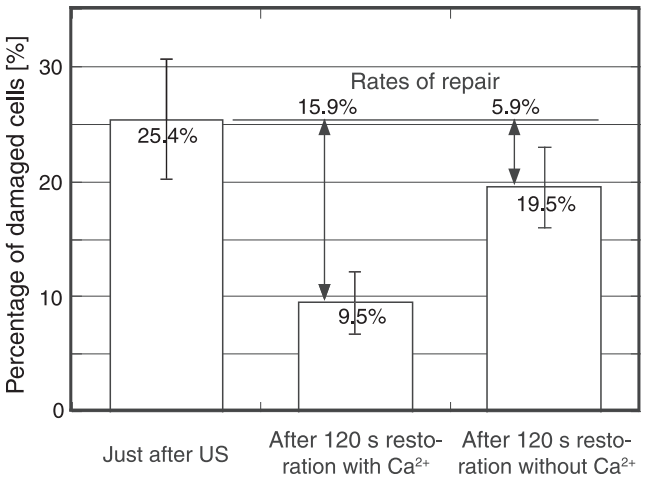

FIGURE 8 The percentage of damaged cells as indicated by PI uptake and fluorescence examined immediately after and 120 s after ultrasound exposure in the presence and absence of Ca^{2+}. Decreases in the damage rates at 120 s after exposure from that immediately after exposure give the rates of repair in the presence and absence of Ca^{2+}.

Two types of bubble behavior, spherical behavior and nonspherical behavior, can result in mechanical effects on cells. At a low intensity of continuous ultrasound, microstreaming produced by gentle oscillation of bubbles with spherical shapes can cause rupture of the cell membrane (35). At a high intensity of ultrasound, symmetric contraction of an inertial cavitation bubble produces a high-pressure shock wave, which is predicted to cause structural change in a lipid bilayer resulting in penetration of water molecules into the cell (36). If bubbles or their surrounding condition have some geometric asymmetry, microjets of a surrounding liquid are produced during bubble collapse. Bjerknes force working between neighboring bubbles or a rigid wall can cause geometric asymmetry, and surface instabilities (37) accelerate distortion in bubble shape.

Ohl et al. (17) used a high-speed camera to observe cell-bubble interaction under exposure to a shock wave of an extracorporeal lithotripter, and they found that a large number of cells detached from a rigid wall during bubble collapse beside the wall. Prentice et al. (16) observed interaction of a cell with a contrast agent bubble located at various distances from the wall and found production of a microjet and resulting membrane perforation of 16 μm in diameter on the cell membrane, which causes lethal damage to the cell. Our study revealed that the occurrence of submicron-sized or smaller microjets resulted in slight membrane damage of ~1 μm in diameter, which is easily repaired within several seconds. In the above studies and our study, cells were incubated on rigid materials, and this condition is very different from that in vivo. However, as shown in our study, microjets estimated from the characteristic shape of bubble fragments were also observed in a direction not against a rigid wall (Fig. 6), indicating that other asymmetries can initiate jetting. Irregularities in bubble shape and shell thickness, interaction between other bubbles, vessel wall, and blood cells may initiate asymmetric bubble behavior.

SEM observation of membrane perforation

SEMs and atomic-force microscopes have been used to observe membrane damage produced during sonoporation (7,16,17,19,38,39). However, their high spatial resolutions are not fully utilized to visualize slight repairable damage. One reason is that cells may have inherent surface structures or artifacts produced during the process for preparation of SEM samples (Fig. 4 and Fig. 5, *e* and *j*). To distinguish slight membrane perforation from these structures and artifacts, preceding confirmation of bubble locations using light microscopy is important. Another reason is that prompt fixation of cells after ultrasound exposure is essential to visualize membrane damage that can easily be restored. In our experiments, the cells were fixed about 5 s after exposure, about the same time as that for completion of membrane repair on average (Fig. 7 *e*), suggesting that the observed cells were in the process of being repaired.

Mechanisms of cell membrane repair

As shown in Fig. 7 *e*, a change in Fura-2 fluorescence was not observed in the control group, which was exposed to ultrasound without bubbles. However, a temporal decrease in Fura-2 fluorescence synchronized with ultrasound exposure was observed in the no-damage group, which was exposed to ultrasound with bubbles. Because PI fluorescence was not observed in either group, the mechanical stress caused by the bubble in the no-damage group might have subtle effects without perforation. The presence of mechanosensitive Ca^{2+} channels in the endothelial cell membrane (40) is a possible explanation for this result. Kumon et al. (41) also used Fura-2 and observed temporal change in intracellular Ca^{2+} under exposure of cells to 0.2-s burst ultrasound with microbubbles. Their results indicated another possibility that calcium waves originating from adjacent perforated cells caused the temporal increase in intracellular Ca^{2+} of nonperforated cells.

During the resealing process in the presence of Ca^{2+}, Fura-2 intensity decreased with a time constant of 2.3 s (Fig. 7 *e*), and transmembrane current of *Xenopus* oocytes was reported to decrease with a time constant of 2.17 s (18). The good agreement in time constants indicates that endothelial cells and oocytes have the same level of inherent ability for rapid membrane repair despite the large difference in their volumes. Occurrence of cell membrane damage depends on the number of bubbles adjacent to each cell. Cell membrane damage was found in 25.4% of the total cells in the experimental condition in which almost all cells have one adjacent bubble, and resealing was found in 15.9% of the total cells, suggesting that ~60% of damaged cells were repaired in our sonoporation method. Though these ratios are still insufficient for practical applications of our

sonoporation method, exposure to several pulses can further improve sonoporation efficiency (15).

CONCLUSIONS

This study showed that a single shot of pulsed ultrasound with a duration of several microseconds is sufficient for perforation of membranes of endothelial cells in the presence of microbubbles attached to the cell membranes. Because this exposure condition is quite different from the condition that produces free radicals, sonochemical effects are not responsible for the observed membrane perforation.

Prompt fixation after ultrasound exposure and SEM observations with preceding information of bubble location made it possible to visualize optically invisible membrane perforations in the process of resealing. The presence of perforations at bubble locations suggests that the perforations were due to a direct mechanical effect of bubble behavior.

The process of microbubble fragmentation during rapid contraction of microbubbles was visualized using a high-speed camera, and production of submicron-sized or smaller microjets was suggested from the characteristic shapes of the fragments. The presence of a micron-sized perforation at a bubble location suggests that the production of microjets is a mechanism by which membrane perforation occurs.

Cell dynamics during membrane resealing was visualized using PI and Fura-2, and occurrence of rapid resealing that is completed within about 5 s was confirmed. Rates of cells with membrane repair were evaluated in the presence and absence of Ca^{2+} in the solution. The higher repair rate in the presence Ca^{2+} suggested that two mechanisms, Ca^{2+}-independent self-sealing of the lipid bilayer and Ca^{2+}-triggered fusion of intracellular vesicles, were both activated during sonoporation.

Under the experimental condition in which almost all cells have one adjacent bubble, 25.4% of the cells were damaged by exposure to single-shot pulsed ultrasound and 15.9% (~60% of the damaged cells) were resealed.

SUPPORTING MATERIAL

Two movies are available at http://www.biophysj.org/biophysj/supplemental/S0006-3495(09)00793-0.

This study was supported by a Grant-in-Aid for Scientific Research from the Japan Society for Promotion of Science and was also carried out under a project of the R & D Group of the Japan Society of Ultrasonics in Medicine.

REFERENCES

1. Bao, S., B. D. Thrall, and D. L. Miller. 1997. Transfection of a reporter plasmid into cultured cells by sonoporation in vitro. *Ultrasound Med. Biol.* 23:953–959.
2. Newman, C. M., A. Lawrie, A. F. Brisken, and D. C. Cumberland. 2001. Ultrasound gene therapy: on the road from concept to reality. *Echocardiography.* 18:339–347.
3. Miller, M. W., D. L. Miller, and A. A. Brayman. 1996. A review of in vitro bioeffects of inertial ultrasonic cavitation from a mechanistic perspective. *Ultrasound Med. Biol.* 22:1131–1154.
4. Miller, D. L., S. V. Pislaru, and J. E. Greenleaf. 2002. Sonoporation: mechanical DNA delivery by ultrasonic cavitation. *Somat. Cell Mol. Genet.* 27:115–134.
5. Greenleaf, W. J., M. E. Bolander, G. Sarkar, M. B. Goldring, and J. F. Greenleaf. 1998. Artificial cavitation nuclei significantly enhance acoustically induced cell transfection. *Ultrasound Med. Biol.* 24: 587–595.
6. Lawrie, A., A. F. Brisken, S. E. Francis, D. C. Cumberland, D. C. Crossman, et al. 2000. Microbubble-enhanced ultrasound for vascular gene delivery. *Gene Ther.* 7:2023–2027.
7. Taniyama, Y., K. Tachibana, K. Hiraoka, T. Namba, K. Yamasaki, et al. 2002. Local delivery of plasmid DNA into rat carotid artery using ultrasound. *Circulation.* 105:1233–1239.
8. Miller, D. L., and J. Quddus. 2000. Sonoporation of monolayer cells by diagnostic ultrasound activation of contrast-agent gas bodies. *Ultrasound Med. Biol.* 26:661–667.
9. Miller, D. L., and J. Quddus. 2001. Lysis and sonoporation of epidermoid and phagocytic monolayer cells by diagnostic ultrasound activation of contrast agent gas bodies. *Ultrasound Med. Biol.* 27:1107–1113.
10. de Jong, N., P. J. Frinking, A. Bouakaz, M. Goorden, T. Schourmans, et al. 2000. Optical imaging of contrast agent microbubbles in an ultrasound field with a 100-MHz camera. *Ultrasound Med. Biol.* 26: 487–492.
11. Ohl, C. D., and R. Ikink. 2003. Shock-wave-induced jetting of micron-size bubbles. *Phys. Rev. Lett.* 90:214502.
12. Postema, M., A. van Wamel, C. T. Lancee, and N. de Jong. 2004. Ultrasound-induced encapsulated microbubble phenomena. *Ultrasound Med. Biol.* 30:827–840.
13. Wolfrum, B., R. Mettin, T. Kurz, and W. Lauterborn. 2002. Observations of pressure-wave-excited contrast agent bubbles in the vicinity of cells. *Appl. Phys. Lett.* 81:5060–5062.
14. van Wamel, A., A. Bouakaz, M. Versluis, and N. de Jong. 2004. Micromanipulation of endothelial cells: ultrasound-microbubble-cell interaction. *Ultrasound Med. Biol.* 30:1255–1258.
15. Okada, K., N. Kudo, K. Niwa, and K. Yamamoto. 2005. A basic study on sonoporation with microbubbles exposed to pulsed ultrasound. *J. Med. Ultrasonics.* 32:3–11.
16. Prentice, P., A. Cuschieri, K. Dholakia, M. Prausnitz, and P. Campbell. 2005. Membrane disruption by optically controlled microbubble cavitation. *Nat. Phys.* 1:107–110.
17. Ohl, C. D., M. Arora, R. Ikink, N. de Jong, M. Versluis, et al. 2006. Sonoporation from jetting cavitation bubbles. *Biophys. J.* 91:4285–4295.
18. Deng, C. X., F. Sieling, H. Pan, and J. Cui. 2004. Ultrasound-induced cell membrane porosity. *Ultrasound Med. Biol.* 30:519–526.
19. Mehier-Humbert, S., T. Bettinger, F. Yan, and R. H. Guy. 2005. Plasma membrane poration induced by ultrasound exposure: implication for drug delivery. *J. Control. Release.* 104:213–222.
20. Humphrey, V. F. 2007. Review ultrasound and matter—physical interactions. *Prog. Biophys. Mol. Biol.* 93:195–211.
21. Inoue, T., and H. Osatake. 1988. A new drying method of biological specimens for scanning electron microscopy: the t-butyl alcohol freeze-drying method. *Arch. Histol. Cytol.* 51:53–59.
22. Karatekin, E., O. Sandre, H. Guitouni, N. Borghi, P. Puech, et al. 2003. Cascades of transient pores in giant vesicles: line tension and transport. *Biophys. J.* 84:1734–1749.
23. Steinhardt, R. A., G. Bi, and J. M. Alderton. 1994. Cell membrane resealing by a vesicular mechanism similar to neurotransmitter release. *Science.* 263:390–393.
24. McNeil, P. L., and R. A. Steinhardt. 1997. Loss, restoration, and maintenance of plasma membrane integrity. *J. Cell Biol.* 137:1–4.
25. McNeil, P. L., and T. Kirchhausen. 2005. An emergency response team for membrane repair. *Nat. Rev. Mol. Cell Biol.* 6:499–505.

26. Olson, H. G., and F. G. Hammitt. 1969. High-speed photographic studies of ultrasonically induced cavitation. *J. Acoust. Soc. Am.* 46:1272–1283.

27. Lauterborn, W. 1982. Cavitation bubble dynamics - new tools for an intricate problem. *Appl. Sci. Res.* 38:165–178.

28. Kudo, N., T. Miyaoka, K. Okada, and K. Yamamoto. 2002. Study on mechanism of cell damage caused by microbubbles exposed to ultrasound. *IEEE Ultrasonics Symp. Proc.* 2:1351–1354.

29. Henglein, A., R. Ulrich, and J. Lilie. 1989. Luminescence and chemical action by pulsed ultrasound. *J. Am. Chem. Soc.* 111:1974–1979.

30. Lawrie, A., A. F. Brisken, S. E. Francis, D. Wyllie, E. Kiss-Toth, et al. 2003. Ultrasound-enhanced transgene expression in vascular cells is not dependent upon cavitation-induced free radicals. *Ultrasound Med. Biol.* 29:1453–1461.

31. Crum, L. A. 1984. Acoustic cavitation series: part five: rectified diffusion. *Ultrasonics.* 22:215–223.

32. Miller, D. L., and A. R. Williams. 1989. Bubble cycling as the explanation of the promotion of ultrasonic cavitation in a rotating tube exposure system. *Ultrasound Med. Biol.* 15:641–648.

33. Christiansen, J. P., B. A. French, A. L. Klibanov, S. Kaul, and J. R. Lindner. 2003. Targeted tissue transfection with ultrasound destruction of plasmid-bearing cationic microbubbles. *Ultrasound Med. Biol.* 29:1759–1767.

34. Leong-Poi, H., J. Christiansen, A. L. Klibanov, S. Kaul, and J. R. Lindner. 2003. Noninvasive assessment of angiogenesis by ultrasound and microbubbles targeted to alpha(v)-integrins. *Circulation.* 107:455–460.

35. Marmottant, P., and S. Hilgenfeldt. 2003. Controlled vesicle deformation and lysis by single oscillating bubbles. *Nature.* 423:153–156.

36. Koshiyama, K., T. Kodama, T. Yano, and S. Fujikawa. 2006. Structural change in lipid bilayers and water penetration induced by shock waves: molecular dynamics simulations. *Biophys. J.* 91:2198–2205.

37. Leighton, T. G. 1997. The Acoustic Bubble. Academic Press, San Diego, CA.

38. Tachibana, K., T. Uchida, K. Ogawa, N. Yamashita, and K. Tamura. 1999. Induction of cell-membrane porosity by ultrasound. *Lancet.* 353:1409.

39. Ross, J. P., X. Cai, J. F. Chiu, J. Yang, and J. Wu. 2002. Optical and atomic force microscopic studies on sonoporation. *J. Acoust. Soc. Am.* 111:1161–1164.

40. Oike, M., G. Droogmans, and B. Nilius. 1994. Mechanosensitive Ca^{2+} transients in endothelial cells from human umbilical vein. *Proc. Natl. Acad. Sci. USA.* 91:2940–2944.

41. Kumon, R. E., M. Aehle, D. Sabens, P. Parikh, D. Kourennyi, et al. 2007. Ultrasound-induced calcium oscillations and waves in Chinese hamster ovary cells in the presence of microbubbles. *Biophys. J.* 93:L29–L31.